Physica B 404 (2009) 2412–2418

Contents lists available at ScienceDirect

Physica B

journal homepage: www.elsevier.com/locate/physb

Crystallization kinetics of Li_2O–PbO–V_2O_5 glasses

Yasser B. Saddeek, Essam R. Shaaban, K.A. Aly *, I.M. Sayed

Physics Department, Faculty of Science, Al-Azhar University, P.O. 71452, Assiut, Egypt

ARTICLE INFO

Article history:
Received 11 January 2009
Received in revised form
14 March 2009
Accepted 29 April 2009

Keywords:
Vanadate glasses
Thermal analysis

ABSTRACT

Lead vanadate glasses of the system $5Li_2O–(45–x)$ PbO–$(50+x)$ V_2O_5, with $x = 0$, 5, 10, and 15 mol% have been prepared and studied by differential scanning calorimetry (DSC). The crystallization kinetics of the glasses were investigated under non-isothermal conditions applying the formal theory of transformations for heterogeneous nucleation to the experimental data obtained by DSC using continuous-heating techniques. In addition, from dependence of the glass-transition temperature (T_g) on the heating rate, the activation energy for the glass transition was derived. Similarly the activation energy of the crystallization process was determined and the crystallization mechanism was characterized. The results reveal the increase of the activation energy for glass transition which was attributed to the increase in the rigidity, the cross-link density and the packing density of these glasses. The phases into which the glass crystallizes have been identified by X-ray diffraction. Diffractograms of the transformed material indicate the presence of microcrystallites of $Li_{0.30}V_2O_5$, $Li_{0.67}O_5V_2$, LiV_6O_{15}, Li_4O_4Pb, and $O_7Pb_2V_2$ in a remaining amorphous matrix.

1. Introduction

In the last decades, attention has been focused on vandate-based glasses in view of their low crystallization tendency, low melting point, good semiconducting properties, high chemical durability, thermal resistivity, etc. which make them an excellent material for memory switching devices. The addition of PbO to any glass system changes the structure of the glass significantly. PbO can be incorporated interstitially in the glass network as a network modifier or network former depending on its content. Also, it can be accommodated in large quantities in oxide glasses, e.g., in silicate and in vanadate binary glasses. The vanadate glasses formed with PbO are quite interesting due to their relatively high electrical conductivity, stability, and wide glass forming range [1–9].

The studies on the structure of binary lead vanadate glasses using several techniques showed that the glass network structure is made up of unaffected VO_5 groups, as in crystalline V_2O_5, and affected VO_5 groups, as in crystalline $Pb(VO_3)_2$, and the lead atoms in these glasses form PbO_3 trigonal pyramids and PbO_4 square pyramids. The types of vanadate anion contained in these glasses consist of $V_2O_7^{4-}$, $(VO_3)_n$ single chains and branched VO_4 and $(V_2O_8)_n$ zigzag chain groups. The fraction of the respective groups depends strongly on the glass composition [10–18]. On the other hand, the semiconducting properties of these glasses are of particular technological importance arising from the hopping of electrons or polarons between two different states (oxidation states) of the transition metal, i.e. V^{4+} or V^{5+}, existing in the vanadate glasses [2,19–21]. Therefore, the interesting properties of promising lead vanadate glasses lead to the present quantitative study of the thermal analysis of $5Li_2O–(45–x)PbO–(50+x)V_2O_5$ with $x = 0$, 5, 10, and 15 mol% glasses.

2. Experimental procedures

The glass samples having the general chemical formula $5Li_2O–(45–x)PbO–(50+x)V_2O_5$ with $x = 0$, 5, 10, and 15 mol% have been prepared by the melt quenching technique [1]. Required quantities of Analar grade Li_2CO_3, PbO, and V_2O_5 were mixed together by grinding the mixture repeatedly to obtain a fine powder. The mixture in approximately 30 g batch was melted in a covered platinum crucible in an electrically heated furnace under ordinary atmospheric conditions at a temperature of about 1123–1173 K (according to PbO content) for 2 h to homogenize the melt. The crucibles were kept covered during melting in order to minimize the volatilization losses. The glass frits were prepared by quenching of glass melts in air. The composition of the obtained samples was in accordance with earlier work [1].

The non-crystalline nature of the annealed glasses was confirmed by X-ray diffraction by using a Philips X-ray diffractometer PW/1710 with Ni-filtered Cu-K_α radiation ($\lambda = 1.542$ Å) operating at 40 kV and 30 mA.

The calorimetric measurements were carried out using a differential scanning calorimeter type Shimadzu 50. The calorimeter

* Corresponding author.
E-mail address: Kamalaly2001@Gmail.com (K.A. Aly).

0921-4526/$ - see front matter © 2009 Published by Elsevier B.V.
doi:10.1016/j.physb.2009.04.051

was calibrated, for each heating rate, using well-known melting temperatures and the melting enthalpies of zinc and indium supplied with the instrument [22,23]. The glass powders weighing 20 mg were contained in an alumina crucible and the reference material was α-alumina powder. The samples were heated in air at heating rates α of 2.5, 5, 10, 20 and 30 K/min. The value of the glass transition, T_g, the extrapolated crystallization onset, T_{in}, and the crystallization peak temperature, T_p, were determined with an accuracy of ±1 K by using the microprocessor of the thermal analyzer.

3. Results and discussion

Fig. 1 represents the XRD patterns for $5Li_2O–(45–x)PbO–(50+x)V_2O_5$ glasses as shown in this figure that the glasses did not reveal discrete or any sharp peaks, but the characteristic broad humps of the amorphous materials.

Fig. 2 shows the DSC traces for DSC thermograms of $5Li_2O–(45–x)PbO–(50+x)V_2O_5$ glasses at heating rate ($\alpha = 20$ K/min). The figure shows an endothermic peak characterizes its glass transition temperature, T_g, and a broad exothermic peak consists of two overlapped crystallized peaks. The heating rate dependence of the characteristic temperatures (T_g and T_p) of $(PbO)_{50}–(V_2O_5)_{50}$ glass (as an example) is shown in Fig. 3. It was noted that as the concentration of V_2O_5 increases, the glass transition temperature increases, and the increase in the heating rate leads to an increase in the characteristic temperatures.

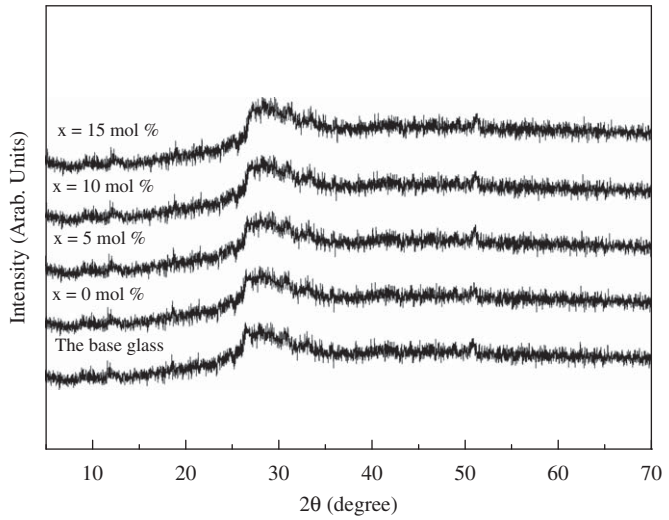

Fig. 1. The X-ray diffraction patterns for $5Li_2O–(45–x)PbO–(50+x)V_2O_5$ ($0 \le x \le 15$ mol%) glass system.

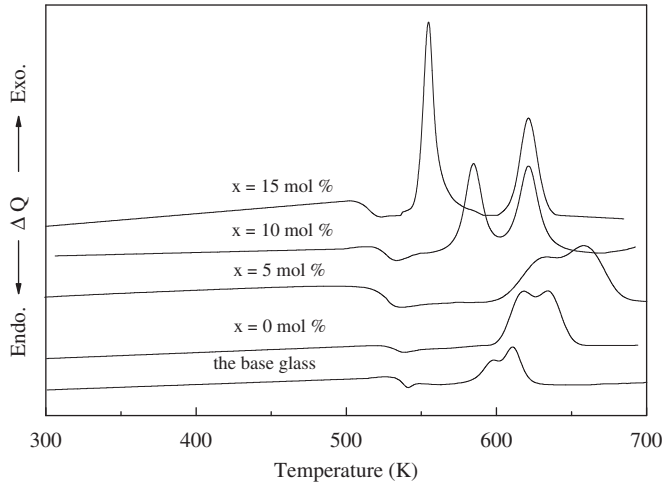

Fig. 2. DSC thermograms for $5Li_2O–(45–x)PbO–(50+x)V_2O_5$ ($0 \le x \le 15$ mol%) glass system at heating rate ($\alpha = 20$ K/min).

3.1. Glass transition

The glass transition temperature dependence on the heating rate (α) can be analyzed by using two methods. The first method uses an empirical relationship in the form

$$T_g = A + B \ln \beta \quad (1)$$

where A and B are constants (tabulated in Table 1) for a given glass composition [24]. Fig. 4 represents the dependence of the glass transition temperature on the heating rate. The obtained results confirm the validity of Eq. (1) for the studied glass system $5Li_2O–(45–x)PbO–(50+x)V_2O_5$ ($0 \le x \le 15$ mol%). The second approach is concerned with the use of Kissinger's formula in the form of [25]

$$\ln(T_g^2/\alpha) = -E_c/RT_g + const. \quad (2)$$

The slope of a straight line between $\ln(T_g^2/\beta)$ and $1/T_g$, as shown in Fig. 5, yields a value of E_g [25], while the values of E_g as function of the V_2O_5 content is shown in Fig. 6. It is noted that the observed increase of E_g is in a good agreement with the increase in the glass transition temperature as the V_2O_5 content increases (see Fig. 4).

On the basis of the thermal studies on the structure of oxide glasses, it has been reported [1,26] that T_g is strictly related to the density of cross-linking, the tightness of packing in the network, the coordination of the network-formers, etc. It has been also

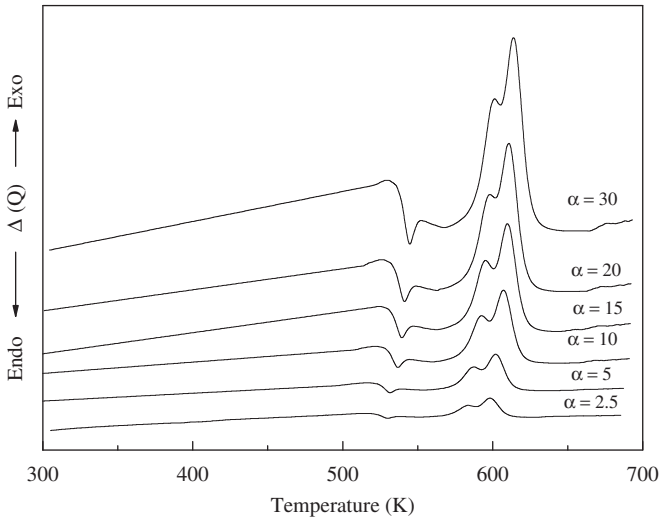

Fig. 3. DSC thermograms for the $50(PbO)–50(V_2O_5)$ glass sample recorded at different heating rates (α in K/min).

Table 1
The A and B constants, the frequency factor K_o and the average value of Avrami's exponent $\langle n \rangle$ for the two crystallization peaks T_{p1} and T_{p2}, respectively, for $5Li_2O–(45–x)PbO–(50+x)V_2O_5$ ($0 \le x \le 15$ mol%) glass system.

X (mol%)	A	B	K_{o1} (S^{-1})	K_{o2} (S^{-1})	$\langle n_1 \rangle$	$\langle n_1 \rangle$
The base glass	528.01	7.32	1.60×10^{27}	3.1×10^{32}	1.391	1.411
0	529.69	7.11	8.20×10^{31}	3.5×10^{43}	1.428	1.439
5	532.67	6.92	3.60×10^{38}	5.9×10^{44}	1.471	1.526
10	534.96	6.65	1.09×10^{34}	4.4×10^{33}	1.594	1.608
15	540.06	6.48	5.9×10^{29}	2.3×10^{25}	1.793	1.817

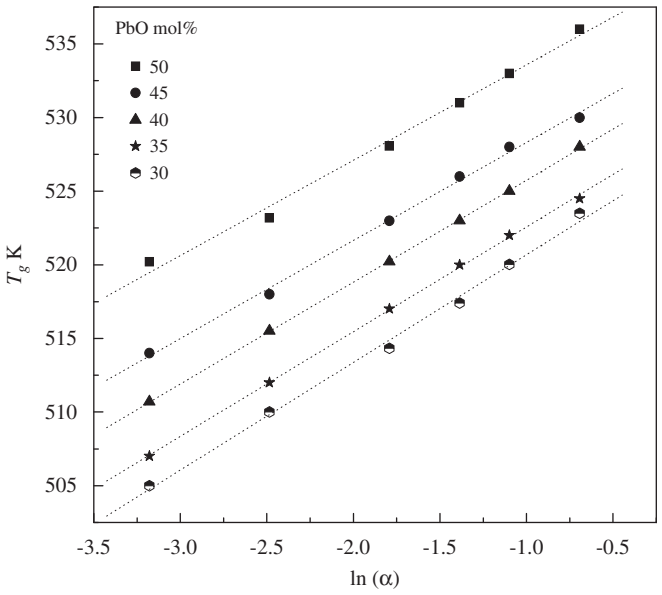

Fig. 4. Glass transition temperature T_g versus ln(α) for $5Li_2O-(45-x)PbO-(50+x)V_2O_5$ ($0 \le x \le 15$ mol%) glass system (α in K/s).

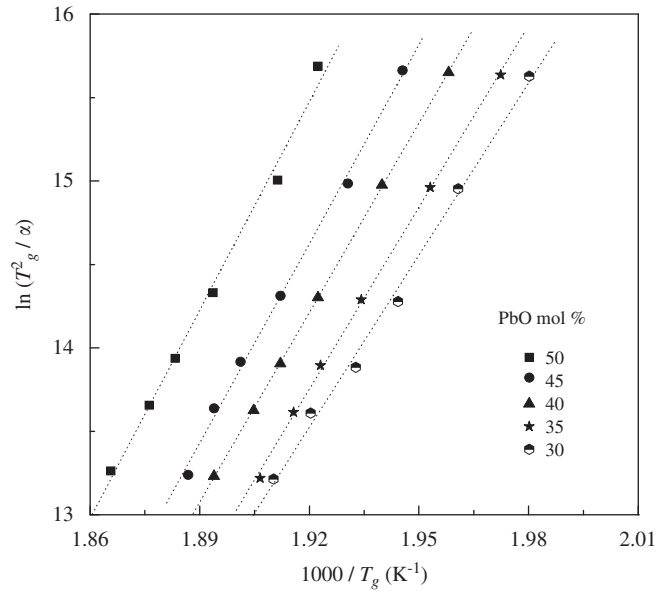

Fig. 5. The plots of $\ln(T_g^2/\alpha)$ vs. $1/T_g$, for $5Li_2O-(45-x)PbO-(50+x)V_2O_5$ ($0 \le x \le 15$ mol%) glass system (α in K/s).

suggested [1] that the density of cross-linking and the molar oxygen volume in the oxide glasses have greater effects on T_g than the bond strength. On the other hand, it is known that the bond length of V_2O_5 with five coordination number is shorter than that of PbO with four coordination number [27]. Thus, the increase in E_g with the increase in V_2O_5 content may be explained as follows: Saddeek et al. [1] in their study on lead vanadate glasses found that the rigidity of these glasses increases as the V_2O_5 content increases as a result of increasing the packing density of the glass system. Also, this increase may be attributed to the higher bond strength of V_2O_5 relative to that of PbO [28], and to the higher cross-linking density in the lead vanadate glasses than in the vitreous V_2O_5. As the V_2O_5 content increases, the cross-link density increases and the non-bridging oxygen will be transformed into bridging oxygen which leads to close packing of the

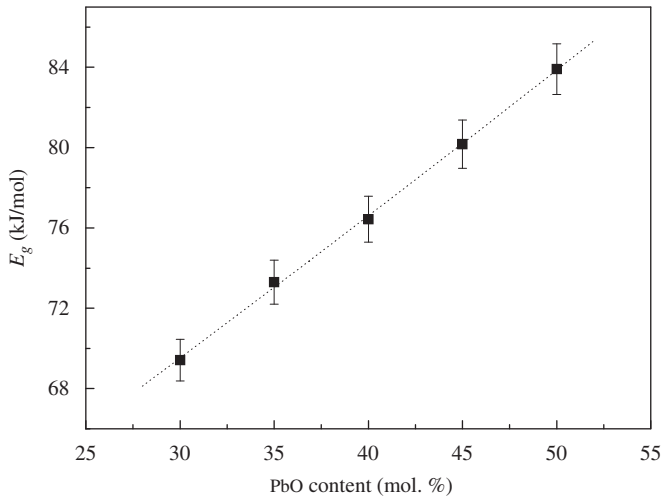

Fig. 6. The average value of the activation energy of glass transition E_g as a function in the V_2O_5 content.

glass network, i.e. the rigidity increases as reported earlier. Thus, the glass matrix will be changed from a two-dimensional layer structure into a more complicated three-dimensional structure, and the average force will increase, which increases the T_g and hence the E_g. The average force constant can be estimated from the relations mentioned earlier [27,29].

3.2. Crystallization kinetics

Fig. 7a depicts the DSC traces of the base glass sample $50(PbO)-50(V_2O_5)$ at $\alpha = 20$ K/min, besides the presentation of the characteristic temperatures such as the glass transition temperature, T_g, and the crystallization peak temperature, T_p. Fig. 7b shows the deconvolution of the two overlapped crystallized peaks, where the indices 1 and 2 in T_{p1} and T_{p2} denote the first peak and the second peak, respectively. The fraction crystallized χ, as shown in Fig. 7c, at a given temperature T, given by $\chi = A_T/A$, where A is the total area of the exothermic peak between the temperatures T_i (the onset of crystallization) and the temperature T_f (the temperature corresponding to full crystallization). A_T is the area between T_i and T. The graphical representation of the crystallized volume fraction shows the typical sigmoid curve as a function of temperature for different heating rates as shown in Fig. 8.

For the evaluation of activation energy for crystallization (E_c) using the variation of T_p with α, Vázquez et al. [30] developed the proposed method by Kissinger [25] for non-isothermal analysis of diversification as follows:

$$\ln[T_p^2/\beta] = E_c/RT_p + \ln(E/RK_0) \quad (3)$$

From the experimental data, a plot of $\ln(T_p^2/\beta)$ versus $1/T_p$ has been drawn for different compositions showing the straight regression line in Figs. 9 and 10 for the two deconvoluted peaks. The activation energy, E_c, and the frequency factor, K_0, can be then evaluated by a least-squares fitting of Eq. (3). The indices 1 and 2 in E_{c1}, E_{c2}, K_{01} and K_{02} denote the first and second peaks, respectively. The values of the activation energy of crystallization obtained for the two peaks are shown in Fig. 11, where the values of the frequency factor were tabulated in Table 1. It is evident that the activation energy for crystallization of the two crystallization peaks increases with the increase in the V_2O_5 content up to 40 mol%, then decreases beyond this value. This variation can be attributed to the larger ionic radii of V^{+5} with respect to that of Pb^{4+} which inhibits crystal formation [27,28].

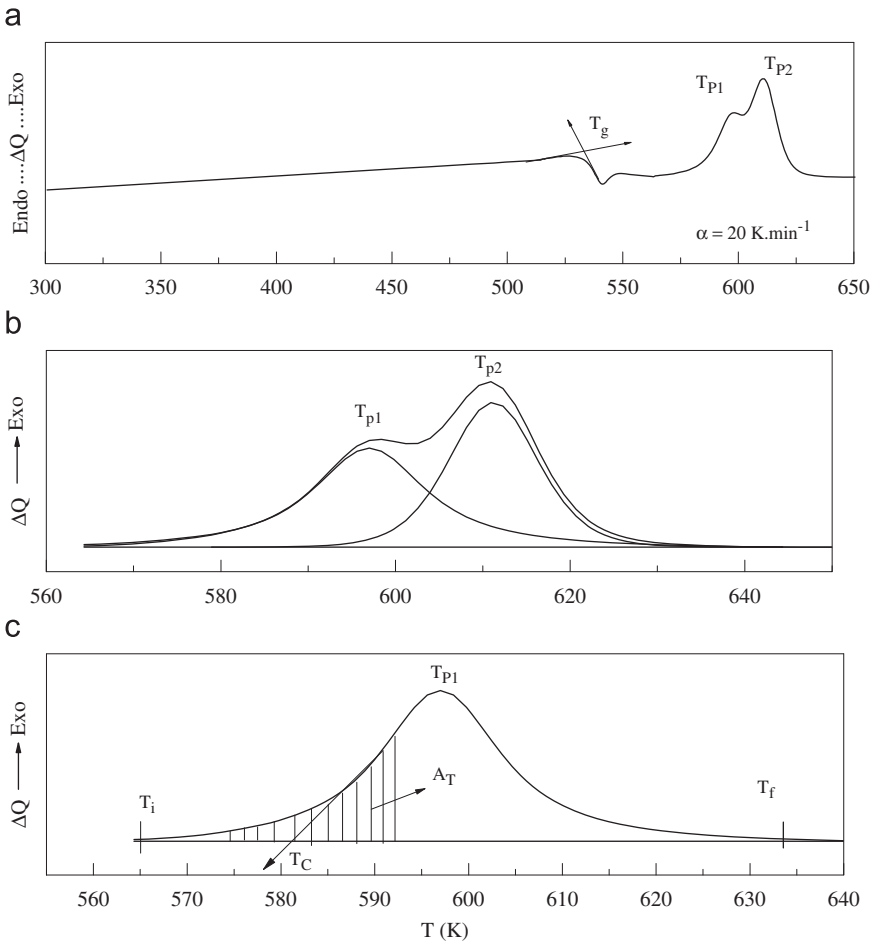

Fig. 7. (a) DSC traces for powdered $50(PbO)-50(V_2O_5)$ glass sample recorded at heating rate 20 K/min, (b) the separation of two overlapped crystallized peaks, and (c) the hatched area shows A_T, which is the area between T_i and T.

The ratio between the ordinates of the DSC curve and the total area of a peak gives the corresponding crystallization rates, which makes it possible to build the curves for the exothermic peaks depicted in Fig. 12. It is found that the values of $(d\chi/dt)_p$ increase with an increase in the heating rate [31–35]. From the experimental values of the $(d\chi/dt)_p$ one can calculate the kinetic exponent n by using the following equation:

$$(d\chi/dt)_p = n(0.37\alpha E_c)/(RT_p^2) \quad (4)$$

Finally, the experimental data of T_p, and $(d\chi/dt)_p$, along with the values of the activation energies of crystallization for the two peaks, according to Figs. 7–11 make it possible to determine, through Eq. (4), the kinetic exponent n, using five experimental heating rates for the two peaks (Table 1). The mean values $\langle n \rangle$ of both the first and second peaks are listed in Table 1. Allowing for experimental error, the value of $\langle n \rangle$ is close to 1.5 for both peaks. The kinetic exponent provides information on the mechanism of crystallization [32–34]. The value of $\langle n \rangle$ for the as-quenched glass is consistent with the mechanism of volume nucleation with two-dimensional growth for both the first and second peaks [32]. It is known that the n values reflect the dimensionality of the structure, with $n = 3$ corresponding to a three-dimensional structure, e.g. SiO_2, $n = 2$, volume nucleation, one-dimensional growth; or $n = 1$, surface nucleation, one-dimensional growth [36]. The increase in n values with increase in V_2O_5 content can therefore be interpreted as a transformation of the one-dimensional vanadate network [33] to a two-dimensional network, which contributes to the decrease in E_c. According to Wells [27], pure crystalline V_2O_5, and hence its amorphous counterpart, has a three-dimensional structure consisting of $[VO_5]$ structural units, as revealed by an n value near 2. This means that crystallization of pure amorphous V_2O_5 involves three-dimensional volume nucleation.

4. Crystallization investigations

To identify the possible phases that crystallize during the thermal treatment applied to the samples, X-ray diffraction patterns were taken for $5Li_2O-(45-x)PbO-(50+x)V_2O_5$ ($0 \le x \le 15$ mol%) glass system at annealed temperatures beyond the first-peak crystallization temperature with a heating rate of 10 K/min for 2 h. The diffractogram of the transformed material after the crystallization process suggests the presence of microcrystallites phases. According to the ICDDVIEW 2006 identification cards [37], these phases can be identified as: (1) lithia vanadate, $Li_{0.30}V_2O_5$, which crystallizes in the monoclinic system with lattice parameters $a = 10.03$ nm, $b = 3.6$ nm, $c = 15.38$ nm, and volume of the unit cell = 519.49 Å^3; (2) lithia vanadate $Li_{0.67}O_5V_2$, which crystallizes in monoclinic system with lattice parameters $a = 15.27$ nm, $b = 3.62$ nm, $c = 10.10$ nm, and volume of the unit cell = 531.44 Å^3; (3) lithia vanadate LiV_6O_{15}, which crystallizes in unknown crystal structure form; (4) lithia lead Li_4O_4Pb which crystallizes in orthorhombic system with lattice parameters $a = 8.31$ nm, $b = 7.30$ nm, $c = 6.52$ nm, and volume of the unit cell = 395.62 Å^3; and (5) lead vanadate $O_7Pb_2V_2$, which crystallizes in monoclinic system with lattice parameters $a = 13.37$ nm, $b = 7.16$ nm, $c = 7.10$

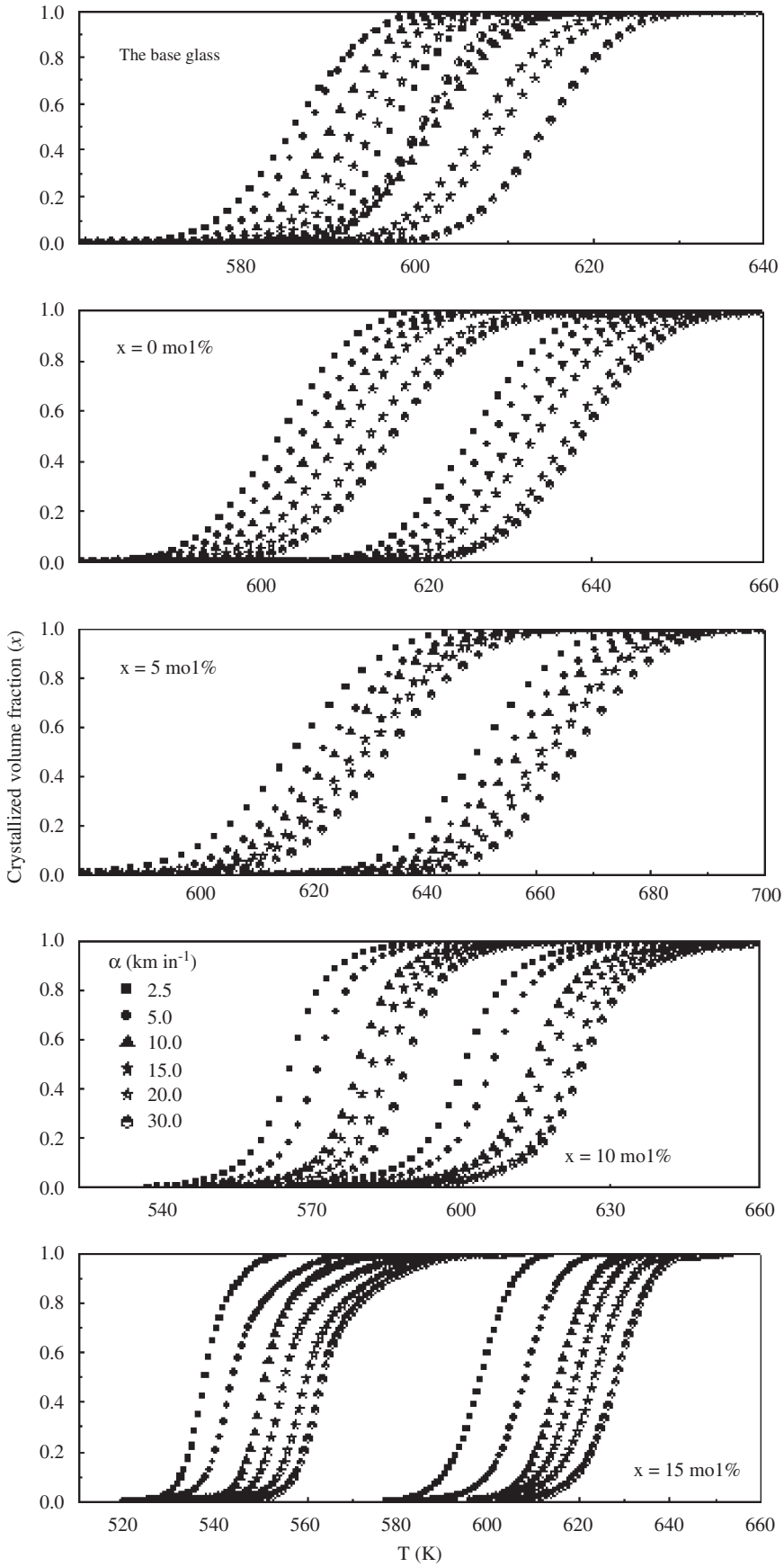

Fig. 8. The crystallized volume fraction (χ) as a function of temperature for $5Li_2O-(45-x)PbO-(50+x)V_2O_5$ ($0 \le x \le 15$ mol%) glasses.

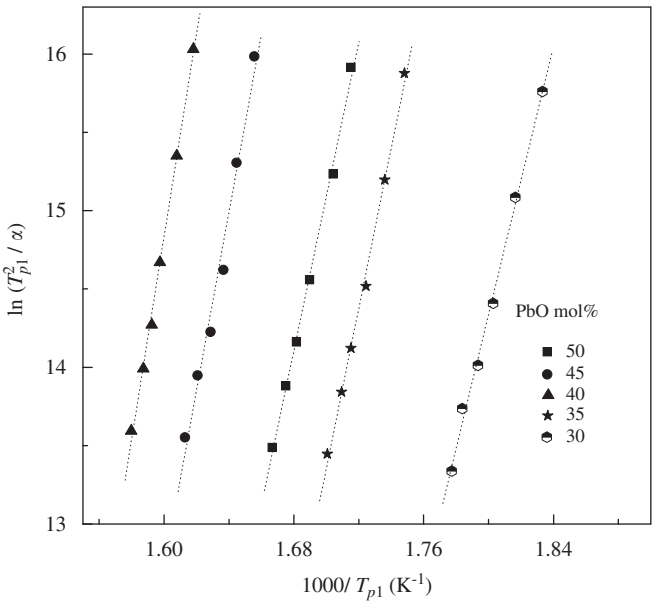

Fig. 9. The plots of $\ln(T_{p1}^2/\alpha)$ vs. $1/T_{p1}$ for $5Li_2O-(45-x)PbO-(50+x)V_2O_5$ ($0 \le x \le 15$ mol%) glass system (α in K/s).

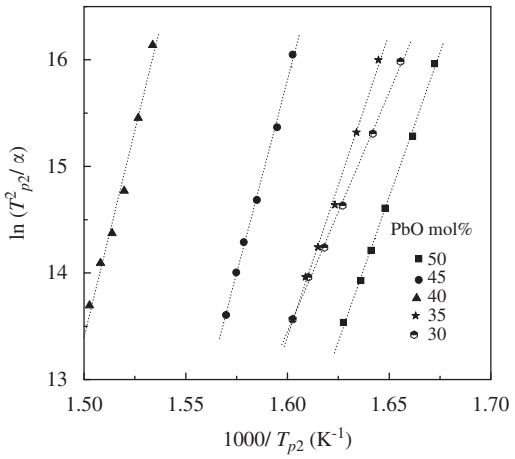

Fig. 10. The plots of $\ln(T_{p2}^2/\alpha)$ vs. $1/T_{p2}$ for $5Li_2O-(45-x)PbO-(50+x)V_2O_5$ ($0 \le x \le 15$ mol%) glass system (α in K/s).

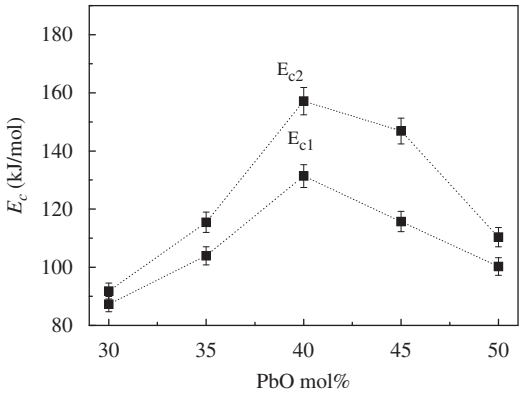

Fig. 11. The activation energy for crystallization E_{c1}, and E_{c2} for $5Li_2O-(45-x)PbO-(50+x)V_2O_5$ ($0 \le x \le 15$ mol%) glass system.

nm, and volume of the unit cell = 653.98 Å^3, respectively. So, the increase in V_2O_5 content in the glasses increases the amount of the $Li_{0.30}V_2O_5$, and $Li_{0.67}O_5V_2$ phases at the expense of the Li_4O_4Pb,

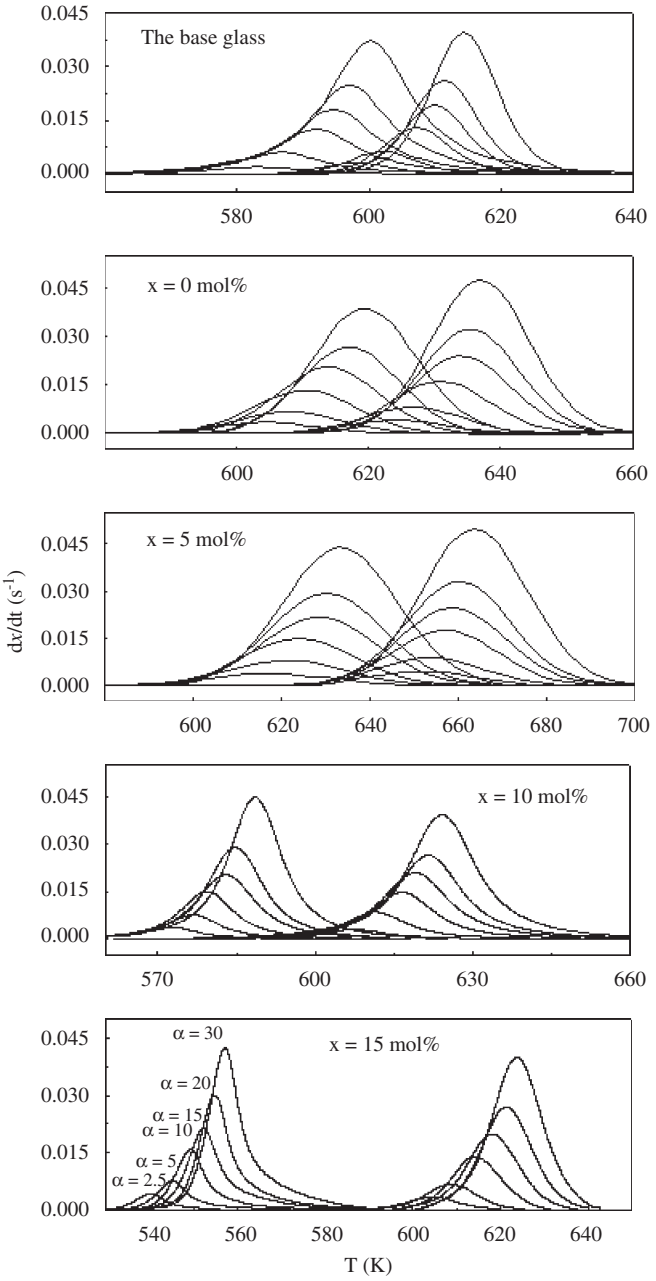

Fig. 12. The crystallization rate ($d\chi/dt$) as a function of temperature for $5Li_2O-(45-x)PbO-(50+x)V_2O_5$ ($0 \le x \le 15$ mol%) glasses.

phase (Fig. 13). This may be the reason for the decrease in E_c, with the suggestion that V_2O_5 inhibiting crystallization. Accordingly, the increase in $O_7Pb_2V_2$ phase may be the reason for the increase in E_g as the dissociation energy of this phase is higher than that of lithia vandate phases. The patterns of the $5Li_2O-(45-x)PbO-(50+x)V_2O_5$ ($0 \le x \le 15$ mol%) samples are almost identical, although there are differences in the intensities between the dominant peaks of each one.

5. Conclusion

The crystallization kinetics of the $5Li_2O-(45-x)PbO-(50+x)V_2O_5$ with $x = 0$, 5, 10, and 15 mol% glasses were investigated under non-isothermal conditions applying the formal theory of transformations for heterogeneous nucleation to the experimental

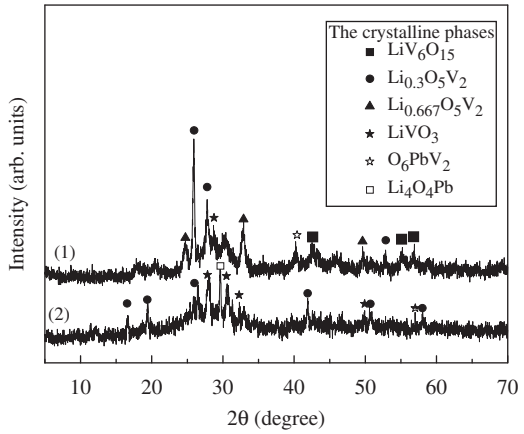

Fig. 13. XRD patterns of crystallized $5Li_2O–45PbO–50V_2O_5$ glass.

data obtained by DSC using continuous-heating techniques. The increase of V_2O_5 content leads to the increase of the activation energy of glass transition as an apparent result of the increase of the glass transition temperature T_g, with increasing V_2O_5 content. The activation energy for crystallization and the numerical factors were investigated and interoperated in terms of the amorphous-crystalline transformations. The phases into which the glass crystallizes have been identified by X-ray diffraction. Diffractograms of the transformed material indicate the presence of microcrystallites of $Li_{0.30}V_2O_5$, $Li_{0.67}O_5V_2$, LiV_6O_{15}, Li_4O_4Pb, and $O_7Pb_2V_2$ in a remaining amorphous matrix.

References

[1] Y.B. Saddeek, E.R. Shaaban, K.A. Aly, I.M. Sayed, J. Alloys Compd. 478 (2009) 447.
[2] J.E. Standworth, J. Soc. Glass. Tech. 36 (1961) 271.
[3] A. Ghosh, B.K. Chaudhuri, J. Non-Cryst. Solids 83 (1986) 151.
[4] M.B. Field, J. Appl. Phys. 40 (1969) 2628.
[5] H. Yamamoto, H. Nasu, J. Matsuoka, K. Kamiya, J. Non-Cryst. Solids 170 (1994) 87.
[6] S. Mukerjee, A. Maiti, U.S. Ghosh, C. Basu, Philos. Mag. B 67 (1993) 823.
[7] M. Sayer, A. Mansingh, Phys. Rev. B 6 (1972) 4629.
[8] H. Hirashima, M. Mitsuhashi, T. Yoshida, Hogykyokai to shi 90 (1982) 411.
[9] H. Hirashima, H. Kurokawa, K. Mizobuchi, T. Yoshida, Glastech. Ber. 61 (1988) 151.
[10] S. Hayakawa, T. Yoko, S. Sakka, J. Ceram. Soc. Japan 102 (1994) 522.
[11] V. Fares, M. Magini, A. Montenero, J. Non-Cryst. Solids 99 (1988) 404.
[12] A.C. Wright, C.A. Yarker, P.A.V. Johnson, J. Non-Cryst. Solids 76 (1985) 333.
[13] S. Mandel, A. Ghosh, Phys. Rev. B 48 (1993) 9388.
[14] S. Hayakawa, T. Yoko, S. Sakka, J. Non-Cryst. Solids 183 (1995) 73.
[15] A. Paul, A. Maiti, C. Basu, J. Appl. Phys. 86 (1999) 3598.
[16] A. Mandal, A. Ghosh, Philos. Mag. B 79 (1999) 1175.
[17] A. Mekki, Arabian J. Sci. Eng. 28 (2003) 73.
[18] V. Rajendran, N. Palanivelu, B. Chaudhuri, K. Goswami, Phys. Stat. Sol. (a) 191 (2002) 445.
[19] N.F. Mott, J. Non-Cryst. Solids 1 (1968) 1.
[20] A. Ghosh, Phys. Rev. B 42 (1990) 5665.
[21] L. Murawski, R.J. Barczynski, J. Non-Cryst. Solids 185 (1995) 84.
[22] DSC-50 Differential Scanning Calorimeter "instruction manual" Simadzu Corporation, 1989.
[23] G.W.H. Höhne, W. Hemminger, H.-J. Flammershiem, Differential Scanning Calorimetry, Springer, Berlin, Heidelberg, 1996.
[24] A. Dahshan, K.A. Aly, M.T. Dessouky, Philos. Mag. 88 (2008) 2399.
[25] H.E. Kissinger, Anal. Chem. 29 (1957) 1702.
[26] J.E. Shebly, J. Appl. Phys. 46 (1975) 193.
[27] A. Wells, Structural Inorganic Chemistry, fourth ed., Clarendon Press, Oxford, 1975.
[28] D. Lide, CRC Handbook of Chemistry and Physics, 84th ed., CRC Press, Boca Raton, FL, 2004.
[29] A. Higazy, B. Bridge, J. Non-Cryst. Solids 72 (1985) 81.
[30] J. Vázquez, C. Wagner, P. Villares, R. Jimenez-Garay, Mater. Chem. Phys. 58 (1999) 187.
[31] P.L. López-Alemany, J. Vázquez, P. Villares, R. Jiménez-Garay, J. Mater. Process. Tech. 143–144 (2003) 866.
[32] S. Mahadevan, A. Giridhar, A.K. Sing, J. Non-Cryst. Solids 88 (1986) 11.
[33] E.R. Shaaban, M. Shapaan, Y.B. Saddeek, J. Phys. Condens. Matter 20 (2008) 155108.
[34] A.A. Othman, K.A. Aly, A.M. Abousehly, Solid State Comm. 138 (2006) 184.
[35] K.A. Aly, A.A. Othman, A.M. Abousehly, J. Alloys Comp. 470 (2009) 574.
[36] A. Goel, E.R. Shaaban, F.C.L. Melo, M.J. Ribeiro, J.M.F. Ferreira, J. Non-Cryst. Solids 353 (2007) 2383.
[37] ICDD View 2006 Release. Cards no. 00-018-0755, 01-074-0054, 01-077-0295, 00-022-0421, 00-024-0668.